Lasers in Manufacturing and Materials Processing
https://doi.org/10.1007/s40516-023-00240-7

RESEARCH

CuCrZr Alloy Manufactured by LPBF Process: Correlation Between Microstructure, Mechanical and Thermal Properties

Carlo Alberto Biffi[1] · Jacopo Fiocchi[1] · Stefano Boldrini[2] · Ausonio Tuissi[1]

Accepted: 15 December 2023

Abstract

Copper based alloys are promising materials for electrical and thermal devices. In this respect, the use of laser powder bed fusion (LPBF) allows the realization of 3D complex structures, possibly enhancing the functional performances of such devices. LPBF also induces refined microstructures and build-up of residual stresses, due to the rapid solidifications and high cooling rate. In this work a CuCrZr alloy was manufactured by LPBF and a process feasibility window was defined. The effect of a heat treatment, consisting of solution annealing and artificial aging, on the microstructure, tensile and thermal properties was evaluated. Moreover, particular attention was addressed to the effect of the building direction on the thermal behaviour. It was found that thermal conductivity is improved by the heat treatment and that thermal conductivity resulted anisotropic, being higher in the growth direction.

Keywords LPBF process · Additive Manufacturing · Cu alloys · Thermal properties · Microstructure

Introduction

Additive manufacturing (AM), also known as 3D printing, is an advanced manufacturing technology, which allows to produce parts from a 3D computer-aided design by building them layer by layer [1]. According to ASTM standard F2792 [2], AM technologies fall into two main categories: Direct Energy Deposition (DED) and Powder Bed Fusion (PBF). The energy source in PBF can be a laser or an electron beam. Nowadays, the laser powder bed fusion (LPBF) process has reached a good maturity and diffusion in the scientific and industrial environments. Particularly,

✉ Carlo Alberto Biffi
carloalberto.biffi@cnr.it

[1] National Research Council of Italy - CNR ICMATE Unit of Lecco, Lecco, Italy

[2] National Research Council of Italy - CNR ICMATE Unit of Padova, Padua, Italy

Published online: 18 January 2024

LPBF systems offer a high number of degrees of freedom in the selection of different process parameters, which need to be identified for the best manufacturing of complex 3D parts [3].

Among the alloys processable by LPBF, Cu and Cu alloys are gaining a large interest for some industrial applications, like heat exchangers for aerospace, automotive, nuclear and energy sectors, thanks to their excellent thermal and electrical properties [4]. New trends in electrical mobility are also pushing a better understanding of the current opportunities in the use of Cu and Cu alloys for advanced devices.

Unfortunately, pure Cu is affected by some issues, as far as LPBF processing is concerned: its high reflectivity in the infrared field, the most typical one for industrial high powder laser systems, makes the laser process very inefficient, and its high thermal conductivity promotes intense heat dissipation during melting. The technological trend for LPBF of Cu alloys suggests to carefully select the proper emission wavelength in ranges where absorption increases [5], or the use of high-power lasers in the infrared field [6]. The adoption of Cu alloys, instead of pure Cu, promotes a better stability of the LPBF process, thanks to the decrease of the thermal conductivity and the increase of the absorption with respect to pure Cu [7–10].

In this light, the CuZrCr alloy is one of the most investigated in the literature, as it displays improved processability with respect to pure Cu, while retaining acceptable thermal properties. Fully-dense CuCrZr samples can be achieved, having as high relative density as 99.5%, with promising mechanical properties [11], and the effect of powder surface modification, aiming at improving laser absorption, have been explored, too [12]. The correlation between the microstructure, typically characterized by columnar grains oriented along the building direction, and thermal and electrical properties have been partially explored in the literature [4, 13–15]. The study of the impact of heat treatments on the microstructure and mechanical properties suggests that a balance between strength, ductility, and thermo-electrical performances can be found and tuned.

In the present work the effect of a heat treatment, based on solution annealing and artificial ageing, on microstructure, tensile properties and thermal conductivity in function of the temperature, was investigated. The effect of the sample orientation on the evolution of the thermal conductivity was also studied.

Experimental

Spherical CuCrZr powder, produced by gas atomization with a mesh size in the 20—63 µm range, was used for studying the feasibility of the LPBF process (Fig. 1). The nominal composition of the powder is reported in Table 1.

A modified Sharebot METALONE system, equipped with a 1 KW continuous wave active fiber laser (1060 nm in emission wavelength) and a galvanometer head from ScanLab, was used to produce prismatic samples (7×7 mm^2 in section) for density measurement and microstructural analyses, plates (xxx) for mechanical testing and disc-shaped samples (12.7 mm in diameter, about 2.5 mm in height) for thermal analysis. Figure 2 shows the positioning of the samples, built on the platform.

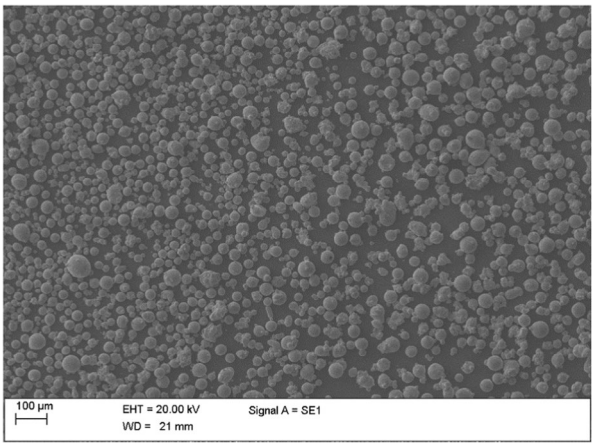

Fig. 1 SEM image of the CuZrCr powder

Table 1 Chemical composition of the CuZrCr powder

	Cr	Zr	Fe	Si	Cu
Nominal composition (wt. %)	0.5–1.2	0.03–0.3	0.08	0.1	Bal

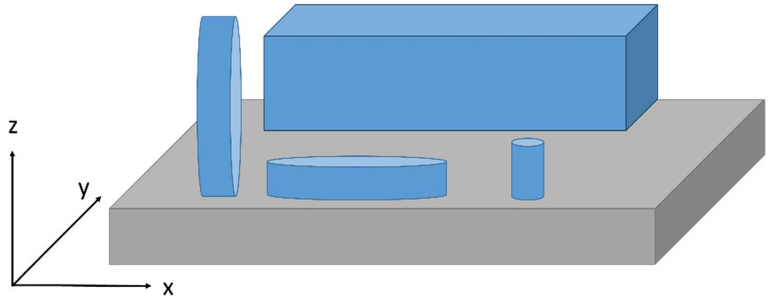

Fig. 2 Schematic of the samples 'manufacturing

The main process parameters, investigated in the present work, are reported in Table 2. A full factorial design was carried out with the aim of maximizing the relative density.

The energy per unit of volume, provided by the laser to the powder bed during LPBF process, is described by the laser fluence (F), and reported in the following [16–18]:

$$\mathrm{F} = \frac{P \cdot t_{ex_P}}{d_p \cdot d_h \cdot s} \tag{1}$$

where P is the laser power, t_{exp} is the exposure time, d_p is the point distance, d_h is the hatch spacing, and s is the layer thickness.

Table 2 Main process parameters used for the LPBF process of the CuZrCr powder

Parameters	Values
Power	380–400-420–440-460–480 W
Scanning speed	500–525-550 mm/s
Scanning strategy	Meander
Atmosphere	Argon
Layer thickness	30 µm
Hatch distance	80 µm
Laser spot size	65 µm
Building plate	Steel

Samples were characterized in the as built and heat treated condition. The investigated heat treatment consisted in a solution annealing (holding at 1000 °C for 1 h followed by water quenching) and an artificial aging (holding at 580 °C for 5 h followed by air cooling). The purpose of heat treatments carried out on LPBFed built samples is typically the homogenization of the microstructure for limiting the anisotropy, for stress relieving and for eventual adjustment of the final properties [4, 11]. In the present case, it is shown that higher thermal conductivity can be obtained after heat treatment.

After the process optimization, three samples in as built condition and three samples in heat treated condition for microstructural, mechanical and thermal characterizations were analyzed.

Density measurements were performed on as built samples by means of Archimede's method on a Gibertini E50S2 precision digital balance. Morphological analysis was carried out using an optical microscope (Leitz Aristomet) on both the xy and the xz sections to reveal the microstructure and defects of the samples in as built and heat treated conditions.

Mechanical testing were performed by an MTS Exceed E45 universal testing machine at room temperature with a strain rate of 3.3 $10-4$ s -1 on dogbone samples, built in the xy plane. The dogbone dimensions were the following: C = 10 mm, B = 15 mm, L = 70 mm, A = 32 mm, T = 1.5 mm, R = 3.5 mm according with the schematic of Fig. 3.

Thermal diffusivity of CuZrCr samples was measured in the 25 – 300 °C range by laser flash method (LFA 457, Netzsch). Cylindrical samples with parallel faces

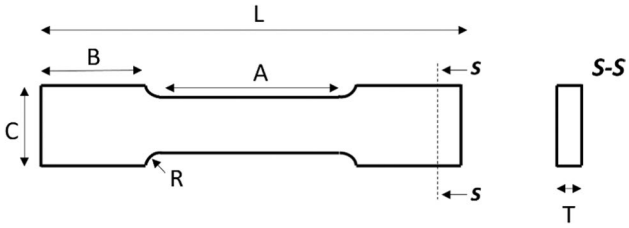

Fig. 3 Schematic of the dogbone sample used for the tensile testing

parallel to XY or XZ planes were graphite coated and specific heat calculated by comparison method using pure iron standard (Netzsch). Thermal conductivity λ was then obtained as $\lambda = \rho c_p \alpha$, where ρ is the density, c_p the specific heat and α the thermal diffusivity. Measurement uncertainty is assumed to be 3% for thermal diffusivity and 7% for thermal conductivity.

Results and Discussion

The feasibility study envisaged the creation of cubic geometry samples for the determination of the best process condition, that would minimize defects, and increase relative density.

Figure 4a shows a representative picture of a matrix of samples, built at varying the investigated process parameters, while Fig. 4b shows the typical evolution of relative density of the built samples as function of laser fluence [16–18]. Lack of fusion defects are obtained for insufficient levels of energy, thus resulting in a low relative density. By increasing the energy irradiated by the laser beam, the melting of the powder bed becomes complete and stable, giving rise to a better powder consolidation and an increase of the corresponding relative density. The highest relative density (99.3%) was achieved at a laser fluence of 345 J/mm^3. By further increasing laser fluence, the temperature of the liquid pool exceeds the proper melting temperature and deep penetration takes place. In this case, the creation of the key-hole induces the generation of gas porosities, which lead to a soft decrease of the relative density of the part [19, 20].

Indeed, the relative density curve is typically characterized by an initial rapid growth of the sample density up to the maximum achievable value, then it softly decreases (see Fig. 4b). Therefore, the choice was done in the selection of the process condition able to offer the maximum relative density value without exceeding with the laser fluence, which could promote the generation of gas pores, due to the key-hole formation.

Therefore, samples produced with laser fluence of 345 J/mm^3, corresponding to power of 440 W and scanning speed of 500 mm/s, will be further characterised with respect to their microstructural and thermal properties.

Some of the built samples underwent solution heat treatment followed by artificial ageing, according with the description reported in the Experimental section. Figure 5 shows the microstructures of as-built and heat treated samples, depicting both xy and xz sections.

As-built samples show a preferential orientation of the crystalline grains along the construction axis, i.e. the vertical one. In fact, the xy view highlights relatively small grains, below 100 µm in size (Fig. 5a), while the xz view shows the elongated grains with lengths of a few hundred microns (Fig. 5b). This indicates that during the LPBF process, columnar growth is favoured, resulting in a strongly anisotropic microstructure. On the contrary, it is not possible to observe the presence of the typical molten pools, linked to the rapid scanning by the laser beam.

The grain size values, measured along both the characteristic directions, the x axis and along the z axis, of the as built and heat-treated samples are reported in

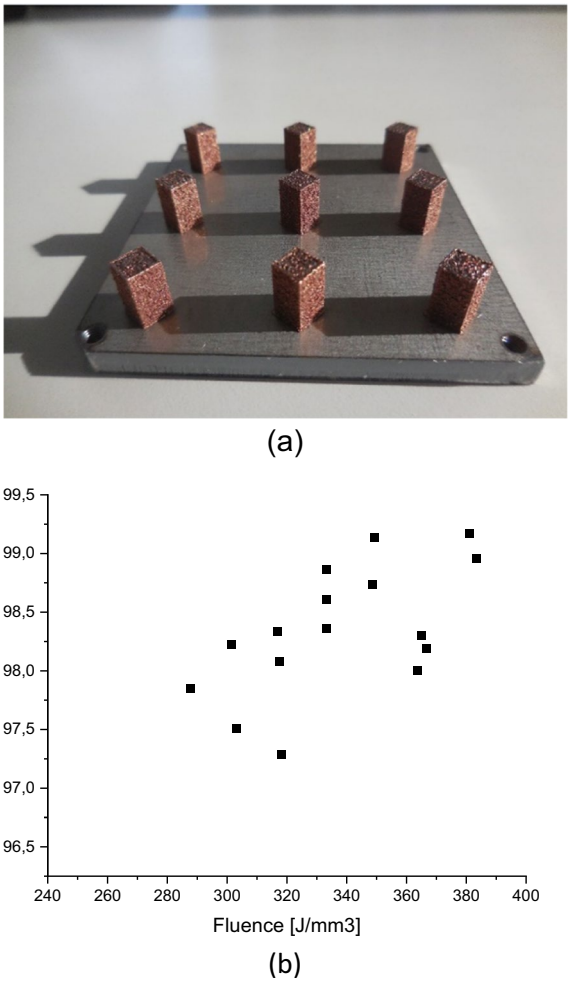

Fig. 4 Representative example of built samples for process mapping (**a**); and relative density versus laser fluence of the built CuZrCr samples (**b**)

Table 3. Heat treatment seems unable to have an evident influence on grain dimension and shape, while its effect can be expected to be more evident at a lower length scale (precipitation and supersaturation).

The corresponding mechanical properties of the specimens in the as-built condition and after heat treatment are reported in Fig. 6. Specimens in the as-built condition exhibit a high elongation to failure (31%) and a tensile strength of 230 MPa. Following the heat treatment, a reduction of the elongation to failure down to 22% is observed, with a slight increase in the ultimate strength up to 265 MPa. The yield stress values in as built and in heat-treaded conditions are 167 and 141 MPa, respectively. The strengthening effect associated to the heat treatment can be explained with different mechanisms for Cu alloys, as reported in literature, such as fine-grain, solid solution, dislocation, and precipitation strengthening [11]. It was found that precipitation strengthening was found to be

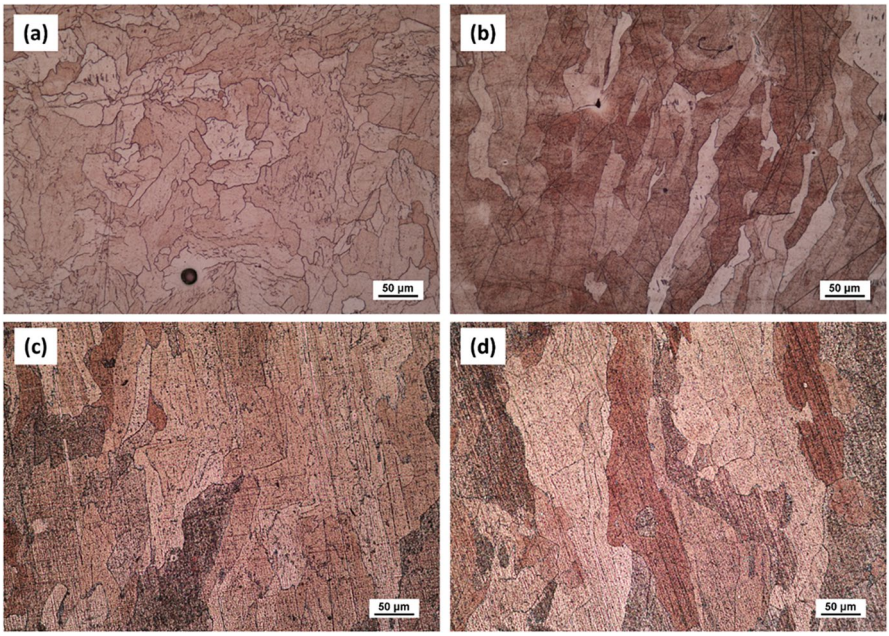

Fig. 5 Optical microscopy images of the CuZrCr samples: xy (**a**) and xz (**b**) views in the as-built condition; xy (**c**) and xz (**d**) views in the heat treated condition

Table 3 Grain size measurements along the x and z axes

Sample condition	Direction	Values [µm]
As-built	x axis	61 ± 22
As-built	z axis	376 ± 120
Heat-treated	x axis	45 ± 28
Heat-treated	z axis	342 ± 72

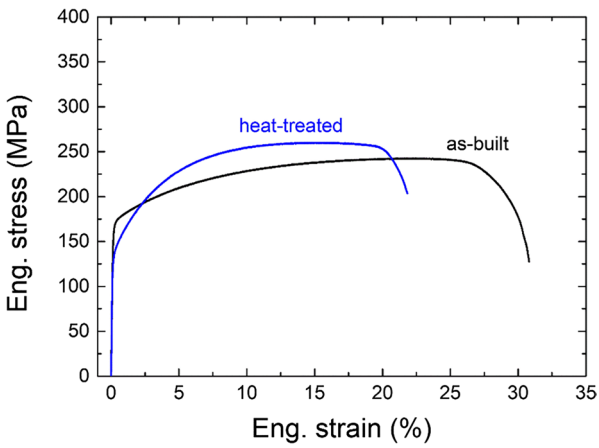

Fig. 6 Stress–strain curves of the CuZrCr samples, built along the xy direction in the as-built and heat treated condition

the main strengthening mechanism of the heat-treated CuCrZr alloy prepared by LPBF [11]. Anyways, some further investigations should be carried out for the validation of this explanation.

The achieved tensile properties of the as-built and heat-treated CuCrZr samples were compared with the wrought alloy: it was verified that larger elongation to failure can be achieved with LPBF process, while the ultimate tensile stress was decreased [21]. These mechanical properties indicate that the material has good ductility, and confirm that residual defects are very limited, if compared with literature [21].

Finally, the thermal conductivity of the CuZrCr samples built in the two main directions was evaluated. Figure 7a-b show the schematic of the built samples and the evolution of thermal conductivity as a function of the temperature in the 25 °C—300 °C range, respectively. Thermal conductivity increases from about 95 W/mK up to 130 W/mK and from about 110 W/mK up to 170 W/mK in as-built samples, built respectively in xy and xz planes. In details, Fig. 7a highlights the axes describing the surface lying on the platform (x and y axis), while z axis indicates the building direction, which is orthogonal to the platform.

This behaviour could depend on the fact that the samples in the as-built condition have a still unstable microstructure and that heating during the measurement can lead to the relaxation of the residual stresses, typical of the LPBF process, and, possibly, to the precipitation of second phases. On the contrary, thermally treated samples oriented along the xz axis show a more constant trend of thermal conductivity, around 350 W/mK, with respect to the temperature increase, while samples oriented along the xy axis exhibit a decrease in thermal conductivity from 345 W/mK down to 300 W/mK.

In any case, it is evident that the building direction influences the thermal conductivity values, but this effect is largely overcome by the effect of heat treatments. In particular, the variation of the thermal conductivity values in function after heat treatment are in good agreement with the ones of the bulk Cu based alloys treated in similar conditions [22].

Conclusions

From the results of the LPBF feasibility map, it can be concluded that the LPBF process allowed to produce dense samples using CuZrCr powder. The tuning of the process parameters allowed to reach relative densities of up to 99.3%. The mechanical characterisation confirmed the good quality of the produced specimens, highlighting elongations to failure of up to 33%, confirming that no significant defects were present in the material.

Following the LPBF process, some specimens were subjected to a heat treatment based on solution treatment and artificial aging, which did not affect grain size. The thermal characterization, performed up to 300 °C, showed that heat treatment could largely improve the thermal properties of the CuCrZr alloy, which are also influenced to a lesser extent by the building direction.

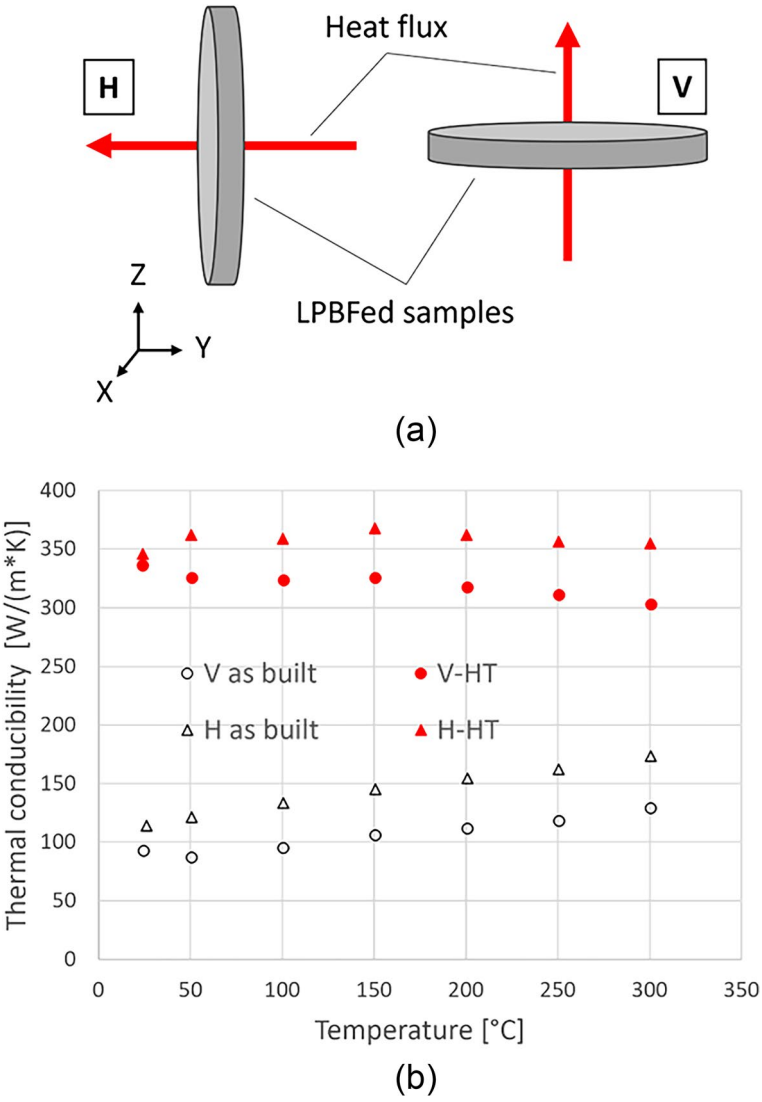

Fig. 7 Schematic of the samples, used for the thermal characterization (**a**), and the evolution of thermal conductivity of the CuZrCr samples, built in xy and xz direction, in the as built condition and after heat treatment (**b**)

Suitable heat treatments are therefore necessary to calibrate the mechanical and thermal performance of copper-based, LPBFed alloy products, in the view of maximizing their functional performance.

Acknowledgements This activity was carried out within the project CUTRED-Sistema Avanzato di Stampa 3D per Scambiatori di Calore in Leghe di Rame—BANDO SI4.0 2020, sponsored by Regione Lombardia. The authors would like to thank Sharebot team and Nicola Bennato from CNR ICMATE for the support in the experimental activity.

Authors' Contributions Biffi wrote the main manuscript and managed the activity.
Fiocchi worked on process optimization and microstructural/mechanical characterization.
Boldrini worked on the thermal characterization.
Tuissi organized the experimental activity.

Funding Open access funding provided by Consiglio Nazionale Delle Ricerche (CNR) within the CRUI-CARE Agreement. The authors did not receive support from any organization for the submitted work.

Data Availability Any datasets used can be accessed by direct request.

Declarations

Ethical Approval None.

Competing Interests The authors declare no competing interests.

References

1. Dowling, L., Kennedy, J., O'Shaughnessy, S., Trimble, D.: A review of critical repeatability and reproducibility issues in powder bed fusion. Mater. Des. **186**, 108346 (2020). https://doi.org/10.1016/j.matdes.2019.108346
2. Standard terminology for additive manufacturing technologies. ASTM Int 2013; F2792–12a.
3. DebRoy, T., Wei, H.L., Zuback, J.S., Mukherjee, T., Elmer, J.W., Milewski, J.O., Beese, A.M., Wilson-Heid, A., De, A., Zhang, W.: Additive manufacturing of metallic components – Process, structure and properties. Prog. Mater Sci. **92**, 112–224 (2018). https://doi.org/10.1016/j.pmatsci.2017.10.001
4. Tang, X., Chen, X., Sun, F., Liu, P., Zhou, H., Fu, S.: The current state of CuCrZr and CuCrNb alloys manufactured bu additive manufacturing: a review. Mater. Des. **224**, 111419 (2022)
5. Singh, A., Caprio, L., Previtali, B., Demir, A.G.: Processability of pure Cu by LPBF using a ns-pulsed green fiber laser. Opt. Laser Technol. **154**, 108310 (2022). https://doi.org/10.1016/j.optlastec.2022.108310
6. Colopi, M., Demir, A.G., Caprio, L., Previtali, B.: Limits and solutions in processing pure Cu via selective laser melting using a high-power single-mode fiber laser. Int. J. Adv. Manuf. Technol. **104**, 2473–2486 (2019)
7. Mao, Z., Zhang, D.Z., Wei, P., Zhang, K.: Manufacturing feasibility and forming properties of Cu-4Sn in selective laser melting. Materials **10**(4), 333 (2017). https://doi.org/10.3390/ma10040333
8. Sabelle, M., Walczak, M., Ramos-Grez, J.: Scanning pattern angle effect on the resulting properties of selective laser sintered monolayers of Cu-Sn-Ni powder. Opt. Lasers Eng. **100**, 1–8 (2018). https://doi.org/10.1016/j.optlaseng.2017.06.028
9. Pogson, S.R., Fox, P., Sutcliffe, C.J., O'Neill, W.: The production of copper parts using DMLR. Rapid Prototyp. J. **9**(5), 334–343 (2003). https://doi.org/10.1108/13552540310502239
10. Grez., J.A.R., Bourell, D.L., Solidification morphology analysis of SLM of Cu powder, Solid Free Form Fabrication Symposium 2004, August 2-4, 2004, Austin, Texas (2004)

11. Wang, Q., Zhang, Y., Wang, K., Liu, S., Zhang, X., Shao, H.: Effect of process parameters and heat treatment on the microstructure and properties of CuCrZr alloy by selective laser melting. Mater. Sci. Eng., A **857**, 144054 (2022)
12. Salvan, C., De Vito, E., Briottet, L., Baffie, T.: Impact of pre-treatments on the surface composition, the optical and flow properties of a CuCrZr powder dedicated to laser powder bed fusion use. Powder Technol. **411**, 117931 (2022)
13. De Terris, T., Baffie, T., Ribière, C.: Additive manufacturing of pure copper: a review and comparison of physical, microstructural, and mechanical properties of samples manufactured with Laser-Powder Bed Fusion (L-PBF), Electron Beam Melting (EBM) and Metal Fused Deposition Modelling (MFDM) technologies. Int. J. Mater. Form. **16**(4), 32 (2023). https://doi.org/10.1007/s12289-023-01755-2
14. Tang, X., Chen, X., Sun, F., Li, L., Liu, P., Zhou, H., Fu, S., Li, A.: A study on the mechanical and electrical properties of high-strenght CuCrZr alloy fabricated using laser powder bed fusion. J. Alloy. Compd. **924**, 166627 (2022)
15 Ma, Z., Zhang, D.Z., Liu, F., Jiang, J., Zhao, M., Zhang, T.: Lattice structures of Cu-Cr-Zr copper alloy by selective laser melting: microstructures, mechanical properties and energy absorption. Mater. Des. **187**, 108406 (2020)
16. Biffi, C.A., Fiocchi, J., Bassani, P., Tuissi, A.: Continuous wave vs pulsed wave laser emission in selective laser melting of AlSi10Mg parts with industrial optimized process parameters : Microstructure and mechanical behaviour. Addit. Manuf. **24**, 639–646 (2018). https://doi.org/10.1016/j.addma.2018.10.021
17 Biffi, C.A., Bassani, P., Fiocchi, J., Albu, M., Tuissi, A.: Selective laser melting of AlCu-TiB2 alloy using pulsed wave laser emission mode: processability, microstructure and mechanical properties. Mater. Des. **204**, 109628 (2021)
18 Biffi, C.A., Fiocchi, J., Valenza, F., Bassani, P., Tuissi, A.: Selective laser melting of NiTi shape memory alloy: processability, microstructure, and superelasticity. Shape Mem. Superelasticity **6**, 342–353 (2020)
19. Shrestha, S., Chou, K.: Formation of keyhole and lack of fusion pores during the laser powder bed fusion process. Manuf. Lett. **32**, 19–23 (2022)
20. Fiocchi, J., Biffi, C.A., Tuissi, A.: Selective laser melting of high-strength primary AlSi9Cu3 alloy: Processability, microstructure, and mechanical properties. Mater. Des. **191**, 108581 (2020)
21. Ma, Z., Zhang, K., Ren, Z., Zhang, D.Z., Tao, G., Haisheng, Xu.: Selective laser melting of Cu–Cr–Zr copper alloy: Parameter optimization, microstructure and mechanical properties. J. Alloy. Compd. **828**, 154350 (2020). https://doi.org/10.1016/j.jallcom.2020.154350
22. METALCOR. http://www.metalcor.de/en/datenblatt/133/